

Scaling properties of two-dimensional turbulence in wakes behind bluff bodies

B. Protas,^{1,2,*} S. Goujon-Durand,^{2,3,†} and J. E. Wesfreid^{3,‡}

¹*Department of Aerodynamics, Institute of Aeronautics and Applied Mechanics, Warsaw University of Technology, ul. Nowowiejska 24, 00-665 Warsaw, Poland*

²*Laboratoire de Physique et Mécanique des Milieux Hétérogènes, CNRS URA 857,*

École Supérieure de Physique et Chimie Industrielles, 10 rue Vauquelin, 75231 Paris Cedex 05, France

³*Faculté de Sciences et Technologie, Université Paris XII-Val de Marne, 61 avenue du Général de Gaulle, 94010 Creteil Cedex, France*

(Received 6 June 1996)

This paper contains an analysis of the scaling properties of two-dimensional (2D) turbulence obtained by means of numerical simulation using the *vortex blob* method. The flow under consideration is the turbulent wake behind a bluff body with a developed enstrophy cascade and reduced inverse energy cascade. The concept of *extended self-similarity* (ESS) and the associated *relative* scaling exponents $\bar{\zeta}_{m,n} = \zeta_n / \zeta_m$ are invoked within the framework of 2D turbulence. The scaling exponents in the enstrophy range are found to systematically vary with the downstream distance from the obstacle, thus revealing their nonuniqueness. In terms of the *relative* exponents, the present results quantitatively agree with recent laboratory experiments of Gaudin *et al.* [PMMH-ESPCI Report No. A 96/57, 1996 (unpublished)]. Error bars and the accuracy of the ESS scaling are carefully checked. [S1063-651X(97)06303-4]

PACS number(s): 47.27.Jv, 47.27.Nz, 47.27.Vf

I. INTRODUCTION

In recent years, new interest has emerged concerning the scaling properties of turbulent flows, e.g., [1,2]. They are reflected in the scale invariance of the Navier-Stokes equations, both in two dimensions and three dimensions [3]. Research is mainly focused on the deviations from the celebrated K41 theory [4]. Usually, they become apparent in the anomalous behavior of the velocity structure functions which are defined in the following way:

$$s_n(r) = \langle [V(x+r) - V(x)]^n \rangle, \quad (1)$$

where r denotes the separation distance, V is the velocity component parallel to r , and $\langle \rangle$ represents the ensemble average. In this respect, in the three-dimensional (3D) case, the K41 theory predicts that the scaling exponent is a linear function of the order of the structure function

$$s_n(r) \sim r^{\zeta_n}, \quad \zeta_n = \frac{n}{3}. \quad (2)$$

On the other hand, in the 2D case, owing to the conservation of both energy and enstrophy, there are two distinct scaling regimes [5]: inverse energy cascade and direct enstrophy cascade. In a number of works, e.g., [6], it has been shown that the values of the ζ_n exponents substantially differ from the predictions of the K41 theory. These anomalies are attributed to the impact of intermittency, i.e., the phenomenon of non-uniform distribution of the velocity increments in the flow field. Therefore, the deviations of the actual values of the

exponents ζ_n from the K41 prediction might be regarded as a measure of the intermittency effects [1].

New possibilities arose when the concept of *extended self-similarity* (ESS) was developed [7]. It states that when one moment is plotted against another, then the scaling is much more pronounced

$$s_n(r) \sim s_m(r) \bar{\zeta}_{m,n}, \quad \bar{\zeta}_{m,n} = \frac{\zeta_n}{\zeta_m}. \quad (3)$$

In other words, the ratio of two scaling exponents (henceforth, denoted by an overbar) stays constant for a wider range of scales than each of them does when taken separately. As was shown in [8], the ESS scaling comprises not only the *inertial range*, but also reaches as far down as a few Kolmogorov scales η . Consequently, the scaling exponents $\bar{\zeta}_{m,n}$ can be computed with much higher accuracy even at relatively moderate Reynolds numbers. Another important feature of ESS is that it provides information in terms of the *relative* scaling exponents $\bar{\zeta}_{m,n}$, which are more universal in that they remain valid also in the 2D case [9]. Thus this concept provides a uniform framework for the investigation of anomalous scaling properties of both 2D and 3D flows. The deviation of the exponent $\bar{\zeta}_n = \bar{\zeta}_{3,n}$ from the linear behavior given by $\bar{\zeta}_n = n/3$ will then be a universal measure of the intermittency independent of the specific scaling properties of the given flow [9]. The differences between the 2D and 3D cases enter only into the determination of the *absolute* exponents

$$\zeta_n = \bar{\zeta}_n \zeta_3. \quad (4)$$

The *absolute* exponent ζ_3 is equal to unity in the 3D homogeneous and isotropic case [1] and in the inverse energy cascade regime in two dimensions, and equal to 3 in the 2D enstrophy cascade regime [10].

*Electronic address: bprotas@meil.pw.edu.pl

†Electronic address: sophie@pmmh.espci.fr

‡Electronic address: wesfreid@pmmh.espci.fr

An interesting problem is how the presence of physically relevant boundary conditions affects the intermittent properties of turbulence and thus the values of the *relative* scaling exponents $\bar{\zeta}_n$. Recently, Gaudin *et al.* [11] performed two series of turbulent wake experiments in two different facilities at the *external* Reynolds numbers (i.e., based on the free stream velocity and the obstacle diameter) equal to 6000 and 12 000. In the following they will be referred to as *experiment I* and *experiment II*, respectively. These experiments show that the $\bar{\zeta}_n$ exponents vary as a function of the downstream distance from the obstacle. Their main result is that the intermittency induced deviations from the K41 theory are much stronger in the near wake than in the far wake. Interaction of the flow with boundaries is responsible for the production of large scale shear and coherent structures. In such cases, substantial degree of anisotropy is introduced at large scales, but locally the flow still remains isotropic. Motivated by these experiments, we hereafter address this set of problems by means of a numerical simulation.

The plan of this paper is as follows. Section II contains a short outline of the *random vortex blob* method that was used in the 2D simulation of the flow. Numerical results pertaining to the problem are presented in Sec. III. A discussion of the results and conclusions are given in Sec. IV.

II. NUMERICAL SIMULATION

In the context of the above-introduced *relative* exponents, it is possible to investigate intermittency in 2D flows in the same way as is done in three dimensions. A numerical simulation of the turbulent wake was performed, in conditions closely resembling those of the experiment (cf. [11]). Usually in the numerical analysis of turbulence pseudospectral methods are used (e.g., [13]). They have the disadvantage, however, that they do not admit any boundary conditions apart from periodic ones. In the present analysis, the *random vortex blob* method was used. It seems particularly well suited to the study of flows where vorticity is concentrated in a limited part of the flow domain (e.g., wakes, shear layers, etc.). Details concerning the formal foundations and implementation of the method can be found in [14–16]. Results of the application of similar methods to the study of the statistical properties of 2D turbulence are presented in [17] and [18]. A brief description of this method is given below.

The *random vortex blob* method is a Lagrangian approach to modeling viscous fluid flow. It is based on the formal similarity between the 2D vorticity equation and the *Fokker-Planck* equation describing evolution of a stochastic Wiener process. Thus the viscous fluid flow may be approximated as the evolution of a family of *vortex blobs* (i.e., small, but finite, vorticity particles). In our simulation, every *vortex blob* is a smeared point vortex with the cutoff parameter (i.e., its diameter) equal to d_B and constant vorticity distribution. Each of them moves according to the stochastic *Ito* equation

$$dx = Vdt + \sqrt{2\nu}dW, \quad (5)$$

where dx is an infinitesimal displacement of a representative Lagrangian vorticity carrier, V denotes the advection (i.e., deterministic) velocity field which is a sum of the potential background flow and interactions with other vortices, dW is



FIG. 1. Snapshot of the vorticity field in the developed wake turbulence. The presented flow domain reaches as far as $48d$ downstream. The two colors represent the regions with positive and negative vorticity. Approximately 10^5 *vortex blobs* are present in the flow field.

an infinitesimal increment of a nonanticipating Wiener process and $\sqrt{2\nu}$ is the amplitude of the Brownian walk with ν representing the coefficient of kinematic viscosity. In every step new vorticity is created in the boundary layer of the obstacle in such a way that the *no-slip* boundary conditions for the velocity field are satisfied. Next, all the *vortex blobs*, both old and new, undergo advection and random walk, their vorticity charges remaining unchanged. The described algorithm does not make use of any eddy viscosity or subgrid modeling.

Using the basic phenomenology [1], one can propose an heuristic argument helping to fix the free parameters of the method: the diameter of the blob d_B should correspond to the viscous cutoff η , the maximum velocity induced by a single *vortex blob*, and the time step of integration should roughly be of the same order of magnitude as the characteristic velocity and the characteristic time for the given length scale (i.e., the length scale of the viscous cutoff η). With these values, the required resolution for the assumed Reynolds number can be achieved. The number of *vortex blobs* used in the simulations was around 10^5 .

III. RESULTS OF THE NUMERICAL SIMULATION

The aim of the numerical simulation was to produce flow conditions similar to those that can be obtained in experiments performed in turbulent wakes behind bluff bodies (of course, as far as this can be achieved within the 2D approximation). The *external* Reynolds number was around 5000. In practice, there were roughly two decades separating the characteristic integral scales from the smallest scales represented by the viscous cutoff η . The flow domain was assumed to be infinite and the obstacle was a circular cylinder. Figure 1 presents a snapshot of the vorticity field in the developed turbulent wake. The next figure (Fig. 2) presents the instan-

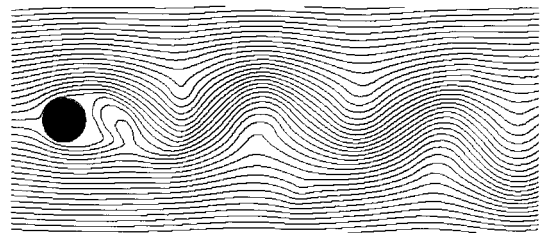


FIG. 2. Instantaneous streamline pattern corresponding to the vorticity field shown above. The presented flow domain reaches $12d$ downstream.

aneous streamline pattern corresponding to the vorticity distribution shown above.

As was mentioned in the Introduction, our attention focused on the *relative* scaling of the structure functions $s_n(r)$. Similarly, as was done in the experiments of Gaudin *et al.* [11], velocity time series were recorded at a number of control points in the wake. All of them were located on the axis, at the following downstream distances from the obstacle: from $2.5d$ to $25d$ every $2.5d$, and from $25d$ to $45d$ every $5d$. Owing to the oscillatory character of the flow in the wake, the direction of the separation vector \vec{r} continually varies in time. Thus the structure functions have to be calculated for the modulus of the velocity vector, rather than for any of its components. Otherwise, the velocity component would not be parallel to the separation vector \vec{r} which would violate definition (1). In order to compute $s_n(r)$, the velocity time series has to be transformed from the time to space domain. Usually this is accomplished by means of the *Taylor hypothesis* [19] which in the presence of big coherent structures is known to give inaccurate results. However, in the case of extended self-similarity the explicit dependence of s_n on r cancels out and therefore the specific form of the $t \rightarrow r$ transformation is irrelevant. In [20] it has been verified that the ESS scaling does not depend on the particular form of the above transformation. Converged statistics could be obtained for low order moments only, therefore we restricted our calculations to $n=2,3,4,6$. So that various time series could be directly compared, all of them were normalized to zero mean and unit normal deviation.

Statistical moments of odd order are characterized by particularly bad convergence properties. This means that in order to obtain reliable results for $n=3$ one needs substantially longer time series than for the case of even orders: $n=2$, $n=4$. It has been established, however [8], that this inconvenience can be overcome when the structure function is calculated with respect to the absolute value of the velocity increment, rather than for the increment itself

$$S_n(r) = \langle [|V(x+r) - V(x)|]^n \rangle. \quad (6)$$

Furthermore, it has been verified in [8] that $S_3(r)$ scales exactly the same as $s_3(r)$. Thus in our ESS analysis we can use $S_3(r)$ instead of $s_3(r)$

$$s_n(r) \sim S_3(r)^{\bar{\zeta}_n}. \quad (7)$$

Figures 3(a) and 3(b) present the scaling of the structure functions $S_n(r)$, $n=2,3,4,6$ versus the separation distance r normalized with respect to the viscous cutoff η . The locations in the wake to which the plots in Figs. 3(a) and 3(b) correspond are $5d$ and $25d$, respectively. It is important to note that for the smallest separations ($r/\eta < 10$) the structure functions have atypical concavity (cf., e.g., [1]). This seems to be an influence of the viscous cutoff d_B and as such ought to be considered a numerical artifact.

As it was already remarked, due to a moderate Reynolds number one can hardly find a range where the slope would remain constant. Therefore, it is not possible to determine the *absolute* scaling exponents with required accuracy. The next plots [Figs. 4(a) and 4(b)] make use of the *extended self-similarity*, i.e., the moments of the structure functions

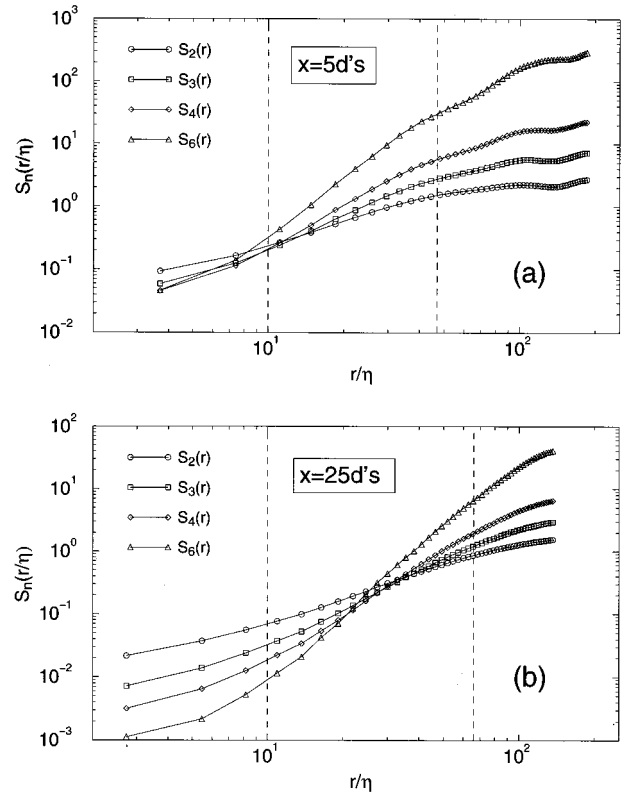


FIG. 3. Scaling of the structure functions $S_n(r)$, $n=2,3,4,6$, vs r/η at the distance: (a) $5d$ and (b) $25d$ downstream from the obstacle; the vertical dashed lines represent the limits of the ESS range.

$S_n(r)$, $n=2,4,6$ are plotted against $S_3(r)$ (only points within the ESS range are shown). The distances from the obstacle are the same as above. The range where the scaling holds is more extensive, the *relative* scaling exponents $\bar{\zeta}_n$ can be determined unambiguously. Close analysis of both *absolute* and *relative* scaling reveals, however, that for bigger separations r/η there is another, rather short and degenerate, scaling regime. In agreement with the properties of 2D turbulent flows [5], it can be identified as the inverse energy cascade. The first scaling regime, shown in Figs. 4(a) and 4(b), represents thus the enstrophy cascade.

Following these lines, the *relative* scaling exponents for the enstrophy range were computed for *all* the control points in the wake. Then for every point related error bars and lengths of the ESS scaling range were estimated. The dependence of the *relative* scaling exponents $\bar{\zeta}_n$ on the downstream distance from the obstacle is shown in Figs. 5–7 for $n=2,4,6$, respectively. This is the central result of the present paper. For comparison, the figures also present the *relative* exponents obtained in the laboratory experiments of Gaudin *et al.* [11], those reported by Benzi *et al.* [8], and the predictions of the She and Leveque theory [12] (for the case of 3D developed isotropic turbulence).

Figure 8 shows error bars for every exponent $\bar{\zeta}_n$, $n=2,4,6$ as a function of the downstream distance from the obstacle. The error bar is defined as the standard deviation of the exponent with respect to the power law fit (7). Related lengths of the ESS range [expressed as the number of pairs $\{S_n(r); S_3(r)\}$ taken into account in the computation

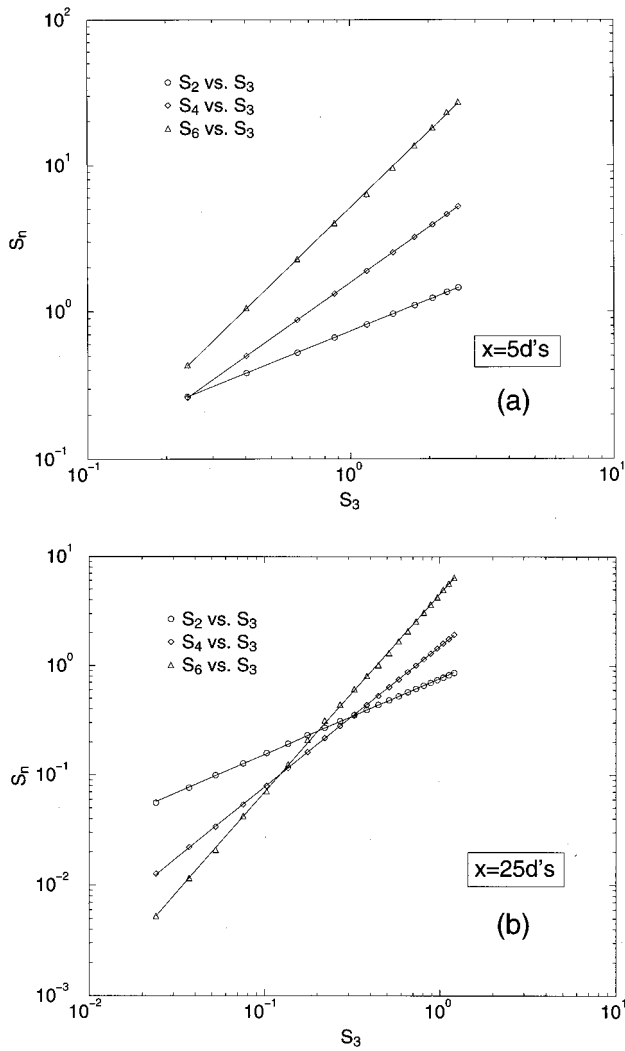


FIG. 4. ESS scaling (enstrophy regime) of the structure functions S_n , $n=2,4,6$, vs S_3 at the distance: (a) $5d$ and (b) $25d$ downstream from the obstacle; continuous lines represent the power law fits.

of the *relative* exponents in the enstrophy range] are presented in Fig. 9. At a given location, the length of the scaling range is the same for all the moments. These two parameters are a measure of the *goodness of the fit* and represent the quality of the scaling.

Great care was taken in order to obtain good quality of the

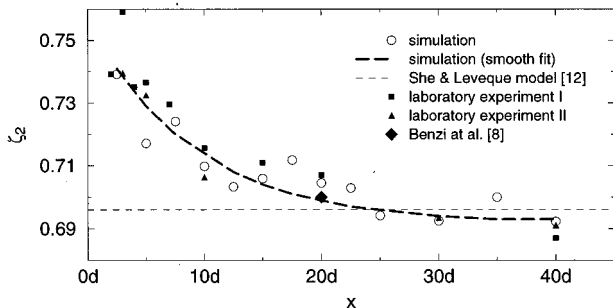


FIG. 5. Dependence of the $\bar{\zeta}_2$ relative scaling exponents on the downstream distance from the obstacle; comparison of the present results with experimental data and theoretical predictions.

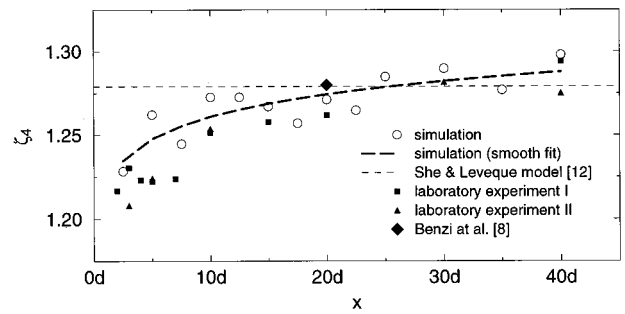


FIG. 6. Dependence of the $\bar{\zeta}_4$ relative scaling exponents on the downstream distance from the obstacle; comparison of the present results with experimental data and theoretical predictions.

scaling. As was earlier found in [6] and [21], the values of the scaling exponents and the related error bars considerably depend on the limits of the range where they are evaluated. Thus it was necessary to define uniform criteria for the determination of the lower and upper bounds of the ESS range in the enstrophy cascade. The lower bound was set equal to a certain multiple of the viscous cutoff length η (in our case it was 10η , comparing to 5η used in [8] and 20η as discussed in [22], both for the 3D case), when the upper bound was taken to be a fraction of the integral scale defined as [23]

$$\Lambda = \frac{1}{b_{LL}(0)} \int_0^\infty b_{LL}(r) dr, \quad (8)$$

where $b_{LL}(r)$ is the longitudinal correlation function for velocity

$$b_{LL}(r) = \langle V(x+r)V(x) \rangle. \quad (9)$$

The fraction of Λ that was taken as the upper limit of the ESS range in the enstrophy cascade was found to slightly vary with the downstream distance from the obstacle.

Consequently, the obtained error bars are relatively low, on the average smaller by one order of magnitude than those reported in [8] and by two orders than those obtained in [9]. This is an important fact, since the variations of the exponents are rather small compared to their average departure from the linear K41 prediction. Thus, in order to bring out these slight variations, a higher accuracy level was required than that which was necessitated by the objectives of the above-cited works.

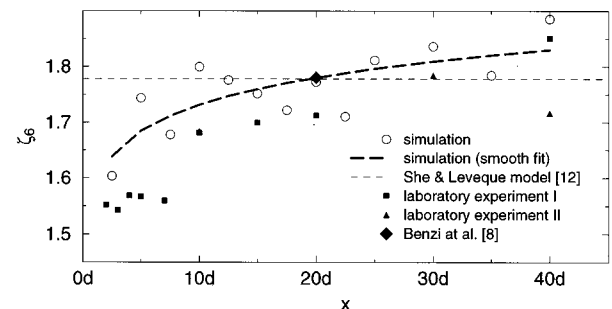


FIG. 7. Dependence of the $\bar{\zeta}_6$ relative scaling exponents on the downstream distance from the obstacle; comparison of the present results with experimental data and theoretical predictions.

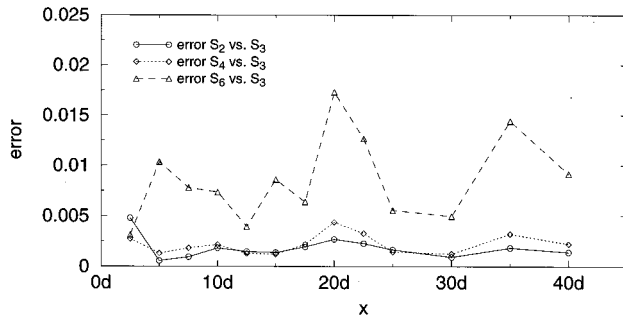


FIG. 8. Values of the error bars for the exponents ζ_n , $n=2,4,6$, as a function of the downstream distance from the obstacle.

IV. DISCUSSION OF THE RESULTS AND CONCLUSIONS

First of all, it ought to be emphasized that in terms of the *relative* scaling exponents ζ_n , the present results obtained in the 2D enstrophy range confirm what we observed in the real 3D laboratory experiments [11]. This is in fact at variance with the statement made in [7] that ESS does not hold in the presence of boundaries where strong shear breaks the large scale homogeneity and isotropy of the flow. Nevertheless, at such locations the length of the ESS scaling range has been found to be shorter. It must be stressed that the present results are compatible with those reported by Benzi *et al.* in [8] which were obtained in 3D turbulent wake at the downstream location of $x=20d$ (cf. Figs. 5–7) at the Reynolds number similar as in [11]. It is visible as one moves downstream that the values of the scaling exponents approach a certain asymptotic limit.

From the collapse of experimental (i.e., 3D) and numerical (i.e., 2D enstrophy cascade) data in Figs. 5–7 it follows that the relative scaling exponents ζ_n , in fact, embody a

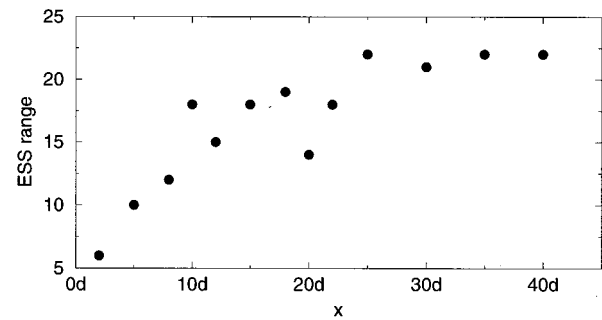


FIG. 9. Length (defined in the text) of the ESS scaling range as a function of the downstream distance from the obstacle.

certain degree of universality with respect to the effects of intermittency in 2D and 3D flows. Another important observation is that the relative scaling exponents are not uniquely determined and independent of the large-scale structure of the flow. Explanation of the discovered anomalies remains an open question. There is some hope however that certain hints may come from the analysis of the topology of the flow patterns in terms of shear and its impact on the stretching of vorticity and vorticity gradients in two and three dimensions, respectively.

ACKNOWLEDGMENTS

B.P. acknowledges the financial support of the French Embassy in Warsaw (Grant CIES No. 160267E) and the hospitality of the PMMH-ESPCI Laboratory. B.P. is also grateful to P. Wald for efficient implementation of the Greengard-Rokhlin algorithm, which considerably enhanced the effectiveness of the numerical simulations. A. Babiano, E. Gaudin, G. Stolovitzky, and J. Wojciechowski are also kindly acknowledged for helpful discussions and assistance.

-
- [1] U. Frisch, *Turbulence: The Legacy of A. N. Kolmogorov* (Cambridge University Press, Cambridge, England, 1995).
- [2] M. Nelkin, *Adv. Phys.* **43**, 143 (1994).
- [3] Ch. R. Doering and J. D. Gibbon, *Applied Analysis of the Navier-Stokes Equations* (Cambridge University Press, Cambridge, England, 1995).
- [4] A. N. Kolmogorov, *C.R. Acad. Sci. URSS* **30**, 301 (1941).
- [5] R. H. Kraichnan and D. Montgomery, *Rep. Prog. Phys.* **43**, 35 (1980).
- [6] F. Anselmet, Y. Gagne, E. J. Hopfinger, and R. A. Antonia, *J. Fluid Mech.* **140**, 63 (1984).
- [7] R. Benzi, S. Ciliberto, C. Baudet, G. R. Chavarria, and R. Tripiccone, *Europhys. Lett.* **24** (4), 275 (1993).
- [8] R. Benzi, S. Ciliberto, C. Baudet, and G. R. Chavarria, *Physica D* **80**, 385 (1995).
- [9] A. Babiano, B. Dubrulle, and P. Frick, *Phys. Rev. E* **52**, 3719 (1995).
- [10] A. Babiano, C. Basdevant, and R. Sadourny, *J. Atmos. Sci.* **42**, 941 (1985).
- [11] E. Gaudin, S. Goujon-Durand, B. Protas, J. Wojciechowski, and J. E. Wesfreid, PMMH-ESPCI Report No. A 96/57, 1996 (unpublished).
- [12] Z. S. She and E. Leveque, *Phys. Rev. Lett.* **72**, 336 (1994).
- [13] A. Vincent and M. Meneguzzi, *J. Fluid Mech.* **225**, 1 (1991).
- [14] A. Chorin, *J. Fluid Mech.* **53**, 785 (1973).
- [15] A. Styczek, *Arch. Mech. Eng.* **XXXIV**, 225 (1987).
- [16] A. Styczek, J. Szumbariski, and P. Wald, *Japanese-Polish Joint Seminar on Advanced Computer Simulation, Tokyo, 1993* (Toranoman Pastiat, Tokyo, 1993).
- [17] J. P. Lynov, A. H. Nielsen, H. L. Pecseli, and J. Juul Rasmussen, *J. Fluid Mech.* **224**, 485 (1991).
- [18] Y. Gagnon, A. Giovannini, and P. Hebrard, *Phys. Fluids A* **5**, 2377 (1993).
- [19] G. I. Taylor, *Proc. R. Soc. London Ser. A* **164**, 476 (1928).
- [20] J.-F. Pinton and R. Labbe, *J. Phys. (France) II* **4**, 1461 (1994).
- [21] G. Stolovitzky and K. R. Sreenivasan, *Phys. Rev. E* **48**, R33 (1993).
- [22] A. Arneodo *et al.*, *Europhys. Lett.* **43**, 411 (1996).
- [23] A. S. Monin and A. M. Yaglom, *Statistical Fluid Mechanics* (MIT Press, Cambridge, MA, 1975), Vol. 2.